

Communication

Interface Modulation of CoNi Alloy Decorated with Few-Layer Reduced Graphene Oxide for High-Efficiency Microwave Absorption

Hai Xie ^{1,2,3}, Jinmei Li ^{1,3,*} , Yaoming Zhang ^{1,3}, Juan Yang ⁴, Tingmei Wang ^{1,2,3} and Qihua Wang ^{1,2,3,*}

¹ Key Laboratory of Science and Technology on Wear and Protection of Materials, Lanzhou Institute of Chemical Physics, Chinese Academy of Sciences, Lanzhou 730000, China; xiehai90@licp.cas.cn (H.X.); yaomingzhang@licp.cas.cn (Y.Z.); tmwang@licp.cas.cn (T.W.)

² Center of Materials Science and Optoelectronics Engineering, University of Chinese Academy of Sciences, Beijing 100049, China

³ State Key Laboratory of Solid Lubrication, Lanzhou Institute of Chemical Physics, Chinese Academy of Sciences, Lanzhou 730000, China

⁴ Laboratory of Clean Energy Chemistry and Materials, State Key Laboratory of Solid Lubrication, Lanzhou Institute of Chemical Physics, Chinese Academy of Sciences, Lanzhou 730000, China; yangjuan@licp.cas.cn

* Correspondence: lijnmei@licp.cas.cn (J.L.); wangqh@licp.cas.cn (Q.W.)

Abstract: Metal-organic frameworks (MOFs)-derived microwave absorbers with tunable components and microstructures show great potential in microwave absorption. Herein, we report a facile thermal reduction approach for synthesizing CoNi alloy/reduced graphene oxide (CoNi/rGO) composites from bimetallic CoNi-MOFs. By tuning the ratio of graphene oxide (GO) in the precursors, the resulting CoNi/rGO-2 composite demonstrates optimal microwave absorption performance with a minimum reflection loss (RL_{\min}) of -66.2 dB at 7.6 GHz in the C band. Moreover, the CoNi/rGO-2 with 50 wt% filler loading achieves a maximum effective absorption bandwidth (EAB) of 6.8 GHz (10.6–17.4 GHz) at a thickness of 2.5 mm, almost spanning the entire Ku band and a portion of the X band. The outstanding performance of CoNi/rGO-2 is ascribed to the high magnetic loss from the CoNi alloy and the incorporation of rGO, which induces interfacial polarization to enhance the dielectric loss and improve the impedance matching of composite. These favorable findings highlight the considerable potential and superiority of the CoNi/rGO-2 composite as an electromagnetic wave absorption material. This work sets forth a viable strategy for designing high-efficiency alloy/rGO absorbers.

Keywords: electromagnetic wave absorption; CoNi alloy; reduced graphene oxide; metal-organic frameworks; reflection loss



Citation: Xie, H.; Li, J.; Zhang, Y.; Yang, J.; Wang, T.; Wang, Q. Interface Modulation of CoNi Alloy Decorated with Few-Layer Reduced Graphene Oxide for High-Efficiency Microwave Absorption. *Coatings* **2024**, *14*, 228. <https://doi.org/10.3390/coatings14020228>

Academic Editor: Alina Pruna

Received: 5 January 2024

Revised: 27 January 2024

Accepted: 12 February 2024

Published: 15 February 2024



Copyright: © 2024 by the authors. Licensee MDPI, Basel, Switzerland. This article is an open access article distributed under the terms and conditions of the Creative Commons Attribution (CC BY) license (<https://creativecommons.org/licenses/by/4.0/>).

1. Introduction

Currently, the severe threat of excess electromagnetic wave pollution and irradiation caused by electronic devices and wireless equipment has garnered significant attention [1–3]. Efforts have been made to improve the impedance matching and attenuation capability of electromagnetic waves, aiming to purify the electromagnetic environment and design superior electromagnetic wave absorbers [4–6]. Therefore, the development of high-efficiency microwave absorption materials with low density, high attenuation intensity, broadband absorption, and strong absorption capacity is deemed urgent for practical applications [7].

In recent years, CoNi alloy has received widespread attention for electromagnetic wave absorption due to its excellent magnetic loss properties and low cost [8–10]. Nevertheless, the high density and mismatching electromagnetic parameters of CoNi alloy hinder its practical application [8,10–12]. Opening up a rational strategy for promoting the microwave absorption performance of CoNi alloy is vital. Lately, metal-organic frames (MOFs) are considered to be an ideal candidate for the preparation of microwave absorption materials

due to their tunable structure, unique pore structure, and excellent electromagnetic coordination and attenuation [13–17]. MOF-derived materials can exhibit high magnetic loss, excellent impedance matching and microwave loss characteristics. For example, Wu et al. prepared nanoporous Co/CoO particles by carbonizing zeolitic imidazolate framework (ZIF)-67, resulting in a minimum reflection loss (RL_{\min}) of approximately -87.2 dB and an effective absorption bandwidth (EAB) of 6.2 [18]. Similarly, Liu et al. pyrolyzed shelled ZIF-67 rhombic dodecahedral cages to prepare hollow Co@N-doped carbon nanocages, achieving an optimal RL_{\min} of -60.6 dB and an EAB of 5.1 GHz at 1.9 mm [19]. Furthermore, graphene, among various carbon-based absorbers, possesses light weight, high electrical conductivity, and remarkable thermal conductivity [20,21]. Nevertheless, the conductivity and electromagnetic parameters of pure graphene are too high to satisfy the impedance matching conditions, which will lead to poor impedance matching conditions and further hinder its practical applications [22]. Therefore, the integration of graphene into MOF-derived alloys is anticipated to enhance impedance matching and induce interfacial polarization to improve dielectric loss.

In this work, MOF-derived CoNi alloy composites decorated with reduced graphene oxide (CoNi/rGO) have been fabricated via a facile thermal reduction method. Encouragingly, the electromagnetic wave absorption properties of CoNi/rGO composites can be improved by adjusting the content of rGO. In addition, benefiting from improved impedance matching and enhanced dielectric dissipation due to the combination of CoNi alloy and rGO, respectively, the optimized CoNi/rGO-2 with a filler loading of 50 wt% can deliver a minimum RL_{\min} of -66.2 dB at 7.6 GHz. Furthermore, the EAB of CoNi/rGO-2 is as large as 6.8 GHz with a thickness of 2.5 mm, covering the range of 10.6–17.4 GHz. Overall, CoNi/rGO-2 exhibits superior electromagnetic wave absorption performance in the low frequency range, providing insights for the preparation of high-efficiency MOF-derived microwave absorbers.

2. Experimental Section

2.1. Synthesis of CoNi-MOF-GO Precursors

The CoNi-MOF-GO precursors were synthesized by the one-pot method. Briefly, 0.02 mol of $\text{Co}(\text{NO}_3)_2 \cdot 6\text{H}_2\text{O}$, 0.02 mol of $\text{Ni}(\text{NO}_3)_2 \cdot 6\text{H}_2\text{O}$ and 20 mg of graphene oxide (GO) were added into 240 mL ethyl alcohol. Then, 2.00 mmol of terephthalic acid (PTA) was added under stirring. Subsequently, the mixed solution was kept at 80 °C for 120 min in an oil bath. After cooling down to room temperature, the solvent was evaporated by rotary evaporation. Finally, the resulting CoNi-MOF-GO was dried at 60 °C for 12 h and marked as CoNi-MOF-GO-1.

For comparison, CoNi-MOF-GO-2 was synthesized in a similar procedure as CoNi-MOF-GO-1, except that the mass of GO was 30 mg. In addition, CoNi-MOF was also prepared by a similar procedure, except that no GO was added.

2.2. Synthesis of CoNi/rGO Composites

The fabrication process of composites is delineated in Figure 1. The CoNi/rGO-1 and CoNi/rGO-2 were prepared by thermal reduction of CoNi-MOF-GO-1 and CoNi-MOF-GO-2 precursors, respectively. Typically, the as-obtained precursors were thermally treated under an atmosphere of 10% H_2 -90% Ar at 600 °C for 4 h with a heating rate of 2 °C min^{-1} . After the pyrolysis process, the CoNi-MOF precursor could be transformed into CoNi alloy, while GO was reduced to rGO. Similarly, the CoNi/C was prepared by pyrolysis of the CoNi-MOF precursor with the same procedure.

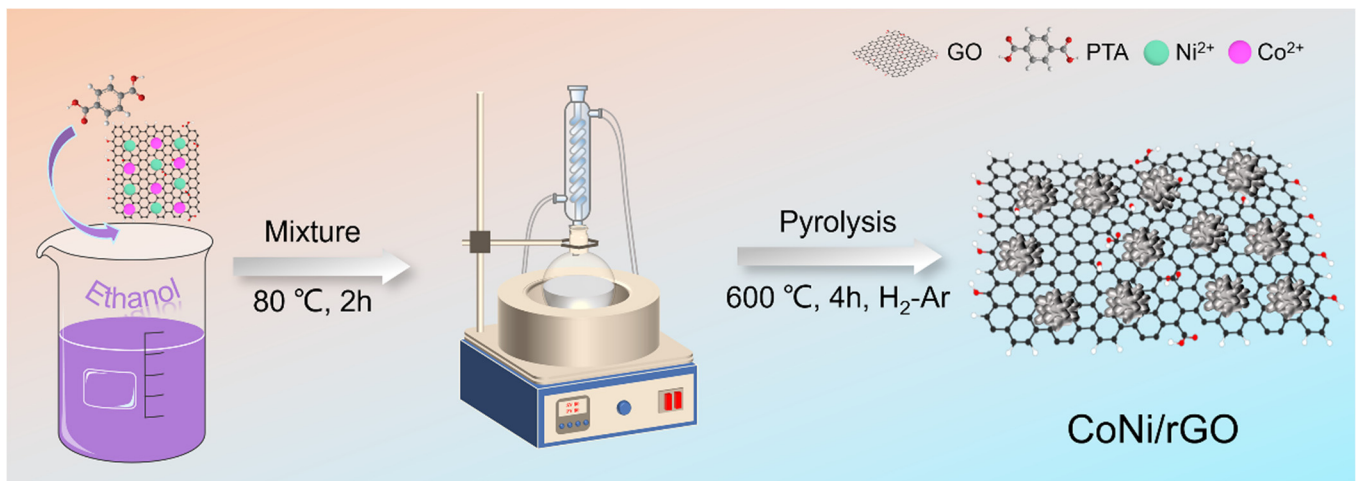


Figure 1. Schematic illustration of the synthesis of CoNi/rGO composites.

2.3. Characterization

Transmission electron microscopy (TEM, JEM-3010, Japan Electron Optics Laboratory, Tokyo, Japan) and scanning electron microscopy (SEM, JSM-6701F, Japan Electron Optics Laboratory, Tokyo, Japan) were performed to investigate the microscopic characterizations and morphology of samples, respectively. X-ray diffraction (XRD, XRD-6100, Shimadzu Corp., Kyoto, Japan) with a Cu K α radiation was carried out to analyze the structural properties of samples. The chemical state and elemental composition of samples were analyzed by the X-ray photoelectron spectroscopy technique (XPS, ESCALAB 250Xi, Thermo Fisher Scientific Inc., Waltham, MA, USA) with an Al K α X-ray source.

2.4. Microwave Absorption and Electromagnetic Parameters Measurement

To detect the electromagnetic parameters of composites, a PNA-L Vector Network Analyzer (Keysight, N5232B, Agilent Technologies, Santa Clara, CA, USA) was conducted over the frequency range of 2–18 GHz. The mixture was prepared by mixing the sample with the molten paraffin (50 wt%). Then, the resultant mixture was pressed into a testing ring with an outer diameter of 7 mm and an inner diameter of 3 mm. The reflection loss (RL) is defined as being a criterion of the absorbed and transmitted power of incident electromagnetic waves [23]. The higher the RL, the higher the absorption. The RL value can be calculated by the complex dielectric constant and permeability according to the transmission line theory [1,24]:

$$Z_{\text{in}} = Z_0 \sqrt{\frac{\mu_r}{\epsilon_r}} \tanh \left[j \left(\frac{2\pi f d}{c} \right) \sqrt{\epsilon_r \mu_r} \right] \quad (1)$$

$$\text{RL (dB)} = 20 \lg \left| \frac{Z_{\text{in}} - Z_0}{Z_{\text{in}} + Z_0} \right| \quad (2)$$

where Z_{in} represents the input impedance, d signifies the thickness of absorber, μ_r is the complex permeability, ϵ_r is the complex permittivity, c is the velocity of light in the free space, Z_0 represents the impedance of free space, and f stands for the frequency of microwave.

3. Results and Discussion

3.1. Material Synthesis and Structural Characterizations

Figure 1 demonstrates the typical preparation process of CoNi/rGO composites. The detailed procedure is outlined in the experimental section. Based on the electromagnetic wave absorption performance, CoNi/rGO-2 was selected as a representative sample for further investigation of its morphology and microstructure using SEM and TEM. As de-

pictured in Figure 2a–c, CoNi/rGO-2 is composed of numerous irregular nanorods decorated with rGO. Following the thermal reduction process, CoNi-MOF is easily transformed into CoNi alloy. Figure 2d illustrates the presence of several irregular nanoparticles on the surface of CoNi alloy. Moreover, a bilayer structure was observed, likely due to the presence of rGO. The high-resolution TEM (HRTEM) image of CoNi/rGO-2 is illustrated in Figure 2e. The inverse fast Fourier transform (IFFT) pattern (as inset in Figure 2e) and the line profile (Figure 2f) reveal a lattice fringe spacing of 0.206 nm, consistent with the (111) plane of $\text{Co}_{0.5}\text{Ni}_{0.5}$ (PDF#04-004-8490), indicating the successful formation of the CoNi alloy. Bright diffraction spots are visible in the selected area electron diffraction (SAED) pattern in Figure 2g, indicating that CoNi/rGO-2 possesses a single crystalline structure. Additionally, elemental mapping images of CoNi/rGO-2 show the uniform distribution of C, O, Co, and Ni elements (Figure 2h).

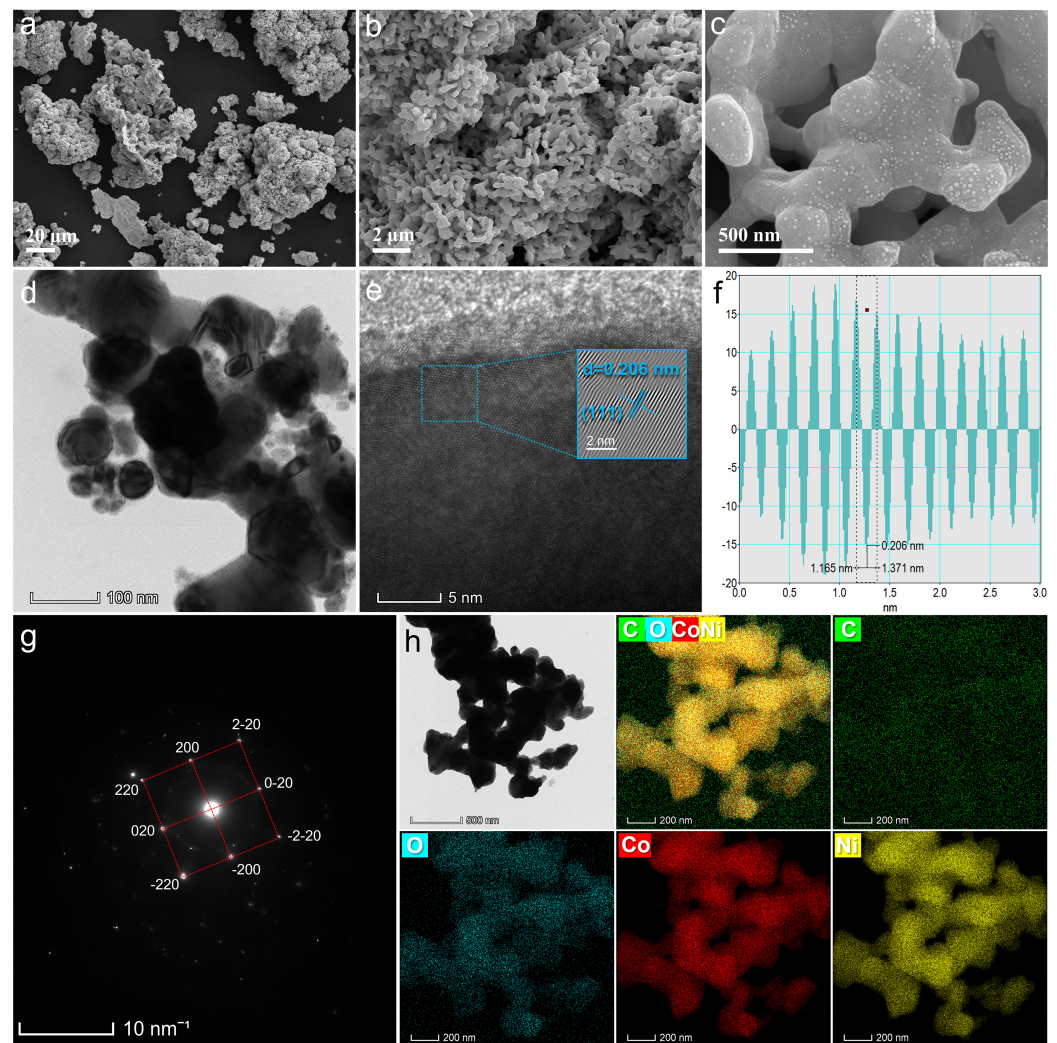


Figure 2. (a–c) SEM images of CoNi/rGO-2. (d) TEM image of CoNi/rGO-2. (e) HRTEM image of CoNi/rGO-2. Inset of (e) is the IFFT pattern. (f) The corresponding line profiles in panel (e). (g) SAED pattern of CoNi/rGO-2. (h) Elemental mapping distributions for C, O, Co, and Ni elements of CoNi/rGO-2.

XRD analysis was conducted on the spectra of CoNi/C, CoNi/rGO-1, and CoNi/rGO-2 to determine the lattice structures of composites. As shown in Figure 3, three distinct diffraction peaks located at 44.4° , 51.7° , and 76.1° are well-associated with the (111), (200), and (220) crystal planes of $\text{Co}_{0.5}\text{Ni}_{0.5}$ (PDF#04-004-8490), respectively. This result indicates the successful formation of the CoNi alloy from CoNi-MOF following a thermal reduction

process, consistent with the TEM results. Furthermore, for CoNi/rGO-1 and CoNi/rGO-2, a wide diffraction peak at 24.0° corresponds to the (002) plane of graphitic carbon [25], demonstrating the effective reduction of GO and the formation of a graphitic structure within the composites [26].

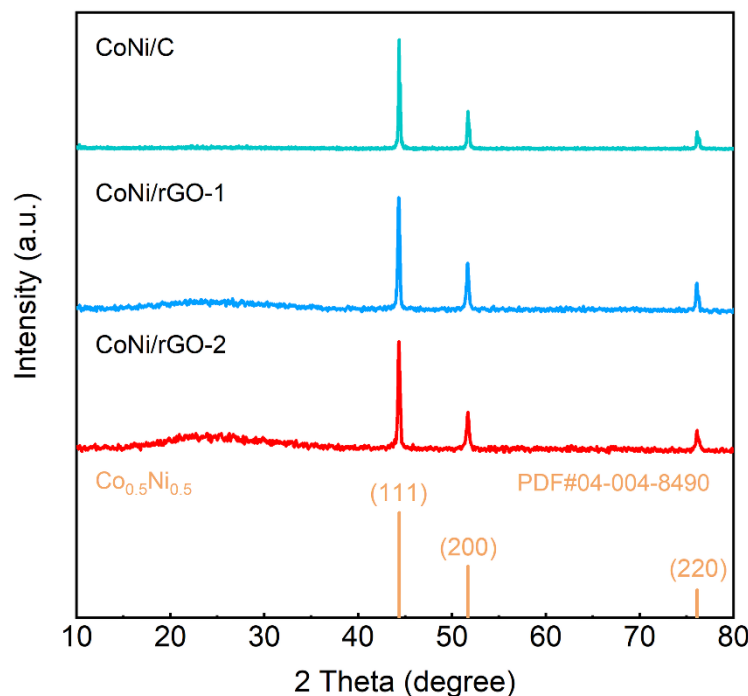


Figure 3. XRD patterns of CoNi/C, CoNi/rGO-1, and CoNi/rGO-2.

To characterize the elemental status and electronic structure of CoNi/C, CoNi/rGO-1, and CoNi/rGO-2 composite, XPS analyses were performed. As shown in Figure 4a, the XPS survey profiles of samples display the signal peaks for C, O, Co, and Ni elements, which is coincident with the elemental mapping result. In the high-resolution C 1s spectra (Figure 4b), the peaks at 284.6 and 285.7 eV can be assigned to the C-C and C-O components, respectively [8,27]. With the introduction of rGO, the C=O peak at 288.2 eV can be observed for CoNi/rGO-1 and CoNi/rGO-2 [8]. As for the Co 2p spectra (Figure 4c), two pairs of doublet peaks are identified at ~ 779.5 and ~ 796.0 eV, corresponding to Co 2p_{3/2} and Co 2p_{1/2}, respectively [28,29]. The high-resolution Co 2p_{3/2} spectra can be fitted with three peaks. The main peaks at 779.3, 781.2, and 786.0 eV are ascribed to the Co⁰, Co²⁺, and satellite signal peaks, respectively [30]. Similarly, in the Ni 2p_{3/2} spectra, there are three primary peaks at 853.2, 855.5, and 861.0 eV, which are assigned to the Ni⁰, Ni²⁺, and satellite species, respectively [31]. The presence of Co⁰ and Ni⁰ species in the complexes demonstrates the successful reduction of CoNi alloys during the thermal reduction process [27,32]. In addition, the existence of Co²⁺ and Ni²⁺ species is caused by the inevitable surface oxidation of the metallic nanoparticles [27,29,33].

3.2. Electromagnetic Wave Absorption Properties of Composites

The RL curves and corresponding 3D/2D RL plots related to the frequency and matching thickness of CoNi/C, CoNi/rGO-1, and CoNi/rGO-2 composites are displayed in Figure 5. It is found that the electromagnetic wave absorption performance of composites can be modulated by changing the ratio of CoNi alloy and rGO. As shown in Figure 5a,d, the CoNi/C with a low thickness of 2.0 mm delivers an RL_{min} value of -50.8 dB at 10.4 GHz. The maximum EAB of CoNi/C is 4.8 GHz (13.0–17.8 GHz) at thickness of 1.5 mm in the X band (Figure 5g). Clearly, the microwave absorption performance of CoNi/rGO-1 and CoNi/rGO-2 is greatly improved via the incorporation of rGO. Specifically, the RL_{min} value of CoNi/rGO-1 reaches -51.9 dB at 6.6 GHz with a thickness of 5.0 mm (Figure 5b,e),

and the corresponding maximum EAB is 5.8 GHz (12.2–18.0 GHz) at 2.5 mm (Figure 5h). Meanwhile, the CoNi/rGO-2 exhibits an RL_{\min} value of -66.2 dB at 7.6 GHz (Figure 5c,f) and a maximum EAB of 6.8 GHz (10.6–17.4 GHz) at 2.5 mm with a filler loading of 50 wt% (Figure 5i), demonstrating that the CoNi/rGO-2 shows potential absorption capability in the low frequency range. As listed in Table 1, the CoNi/rGO-2 demonstrates excellent electromagnetic wave absorption performance and broad EAB, surpassing many other reported MOF-based absorbers. This outcome indicates the potential use of CoNi/rGO-2 as a promising microwave absorber. The enhanced performance can be ascribed to the introduction of numerous structural defects of graphene in CoNi/rGO-2, which induce more permanent electric dipoles and thereby improve dielectric loss [34].

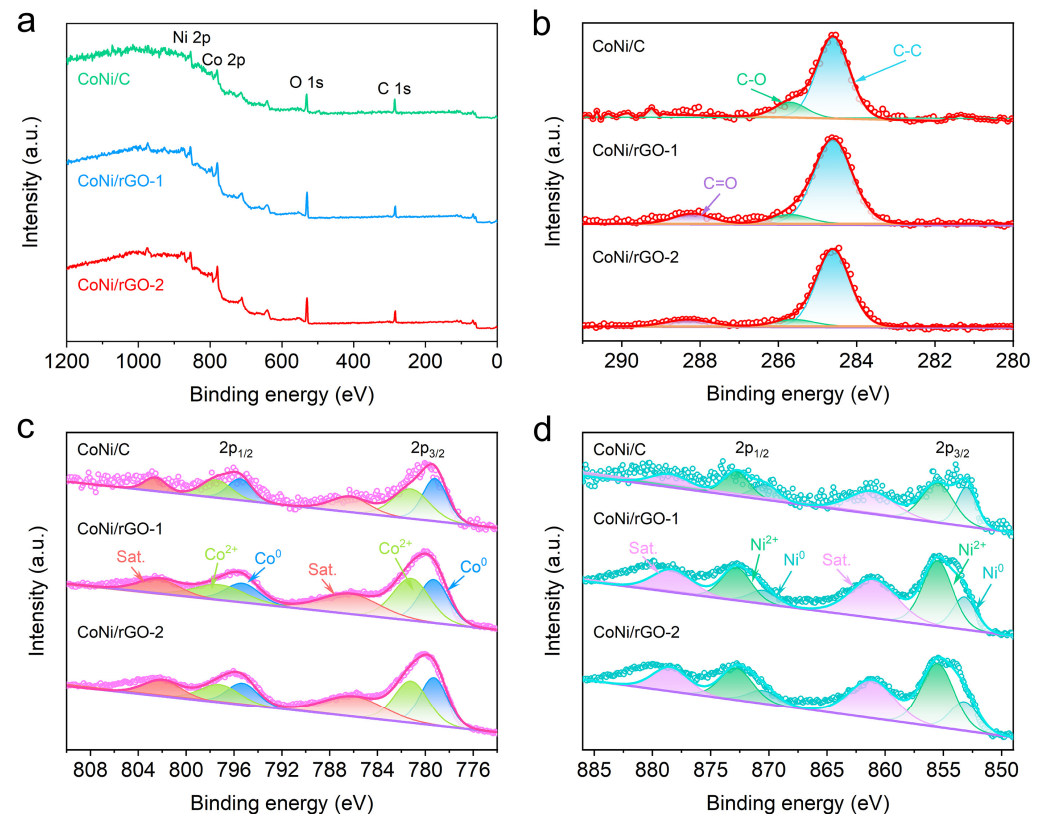


Figure 4. XPS spectra of CoNi/C, CoNi/rGO-1, and CoNi/rGO-2 composites. (a) XPS survey spectra. (b) High-resolution C 1s spectra. (c) High-resolution Co 2p spectra. (d) High-resolution Ni 2p spectra.

Table 1. Comparison of electromagnetic wave absorption properties with various MOF-based absorbers.

Absorbers	Matching EAB (GHz)	RL_{\min} (dB)	References
Cu-S-MOF	6.72 (9.68–16.4)	-52.8	[35]
Co-C composite	6.1 (14.6–8.5)	-48.5	[36]
DM-700-3	2.0 (5.0–7.0)	-67.5	[37]
CoFe@C	9.2 (8.8–18.0)	-61.8	[38]
Ni-MOF@N-C-500	6.8	-69.6	[39]
CNT/FeCoNi@C	6.0	-51.7	[40]
DM-700	4.8	-65.2	[41]
CoZn/C@MoS ₂ @PPy	4.56	-49.18	[42]
Ni@C@ZnO	4.1	-55.8	[43]
Co/Co ₃ O ₄ @HCNs	6.6	-50.6	[44]
CoNi/rGO-2	6.8 (10.6–17.4)	-66.2	This work

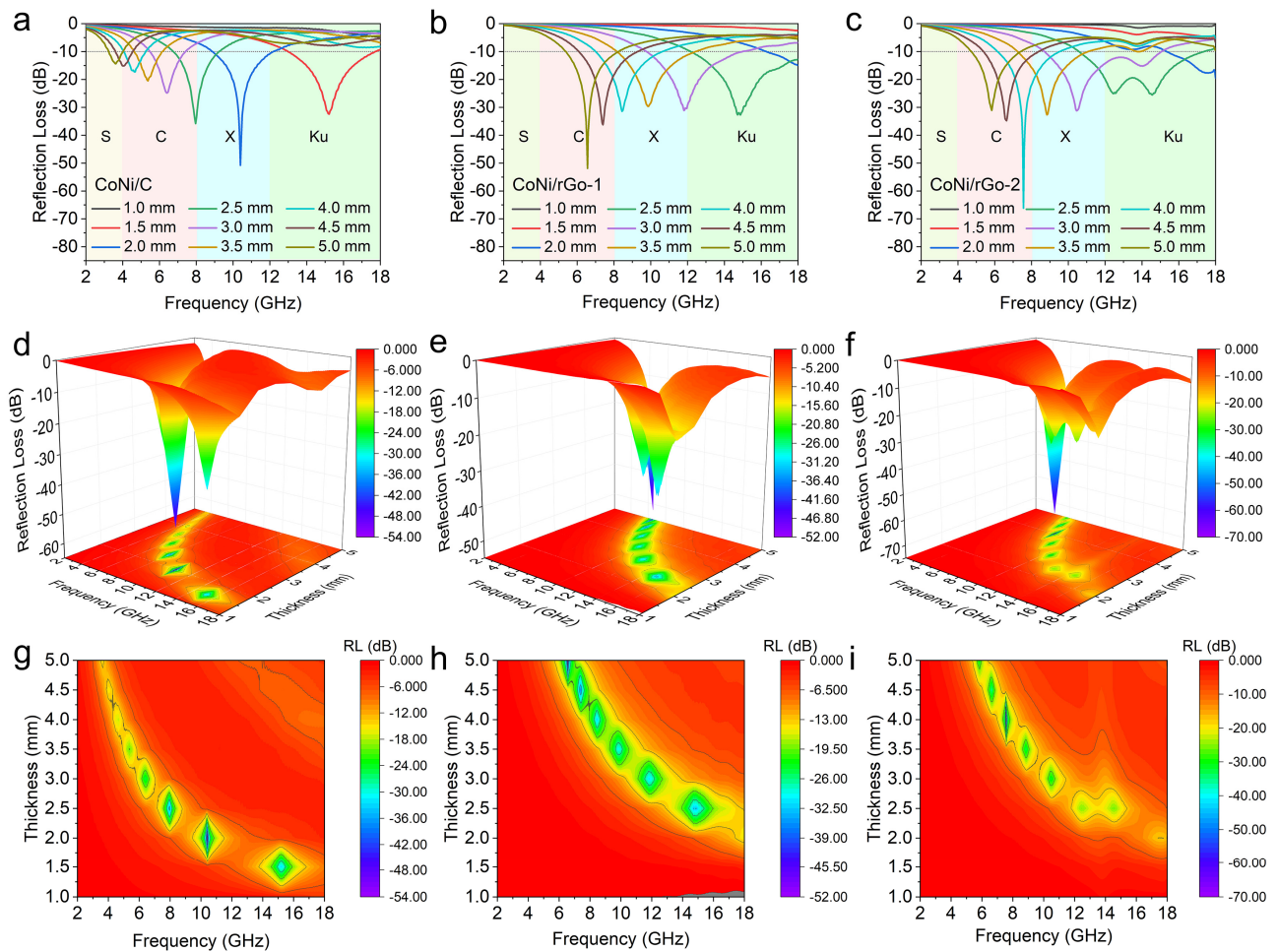


Figure 5. Frequency dependence of RL curves at different thicknesses of (a) CoNi/C, (b) CoNi/rGO-1, and (c) CoNi/rGO-2. The calculated 3D plots of RL for (d) CoNi/C, (e) CoNi/rGO-1, and (f) CoNi/rGO-2. The corresponding 2D plots of RL for (g) CoNi/C, (h) CoNi/rGO-1, and (i) CoNi/rGO-2.

To understand the electromagnetic wave absorption capabilities of CoNi/C, CoNi/rGO-1, and CoNi/rGO-2, the relationships between frequency and different electromagnetic parameters were examined. Generally, the real parts of complex permittivity (ϵ') and permeability (μ') represent the storage ability of electric field energy and magnetic energy, respectively [45]. The imaginary parts of complex permittivity (ϵ'') and permeability (μ'') represent the corresponding loss capacity [17]. The microwave absorption property of samples is primarily related to their complex permittivity ($\epsilon_r = \epsilon_r' - j\epsilon_r''$) and complex permeability ($\mu_r = \mu_r' - j\mu_r''$) [46]. As shown in Figure 6a, the ϵ' values of CoNi/C, CoNi/rGO-1, and CoNi/rGO-2 decrease from 12.8 to 10.4, 6.5 to 4.5, and 7.2 to 4.7, respectively, indicating that the ϵ' values show a decreasing trend with the increase of the frequency due to the dispersion behavior induced by the polarization lag [47]. In addition, the ϵ'' values of CoNi/C, CoNi/rGO-1, and CoNi/rGO-2 change from 0.3 to 2.0, 4.8 to 3.2, and 5.1 to 2.3, respectively (Figure 6b). The presence of resonance peaks is attributed to the existence of multi-polarization process [27]. The rise in dielectric loss of CoNi/rGO-1 and CoNi/rGO-2 at low frequency compared to CoNi/C indicates an increase in their electrical conductivity, further suggesting that the introduction of rGO is contributed to hopping conductivity losses [17]. The dielectric dissipation capacity of composites is further evaluated by dielectric loss tangent ($\tan\delta_\epsilon = \epsilon''/\epsilon'$). As depicted in Figure 6c, the CoNi/rGO-1 and CoNi/rGO-2 exhibit higher $\tan\delta_\epsilon$ values than CoNi/C, demonstrating that CoNi/rGO-1 and CoNi/rGO-2 have stronger dielectric loss [27], which is due to the fact that rGO can

induce more permanent electric dipoles [34]. Furthermore, it can be seen that both the μ' and μ'' values of CoNi/rGO-1 and CoNi/rGO-2 show low values compared with ϵ' and ϵ'' (Figure 6d,e), which may be related to lower content of magnetic component. As shown in Figure 6f, the magnetic loss tangent ($\tan\delta_\mu = \mu''/\mu'$) values of CoNi/C, CoNi/rGO-1, and CoNi/rGO-2 show a similar trend to those of μ'' values. Meanwhile, for CoNi/rGO-1 and CoNi/rGO-2, the $\tan\delta_\epsilon$ values are significantly higher than $\tan\delta_\mu$ values. This improvement may be attributed to relaxation and polarization from the defects and functional groups of rGO, resulting in remarkable dielectric loss ability [48].

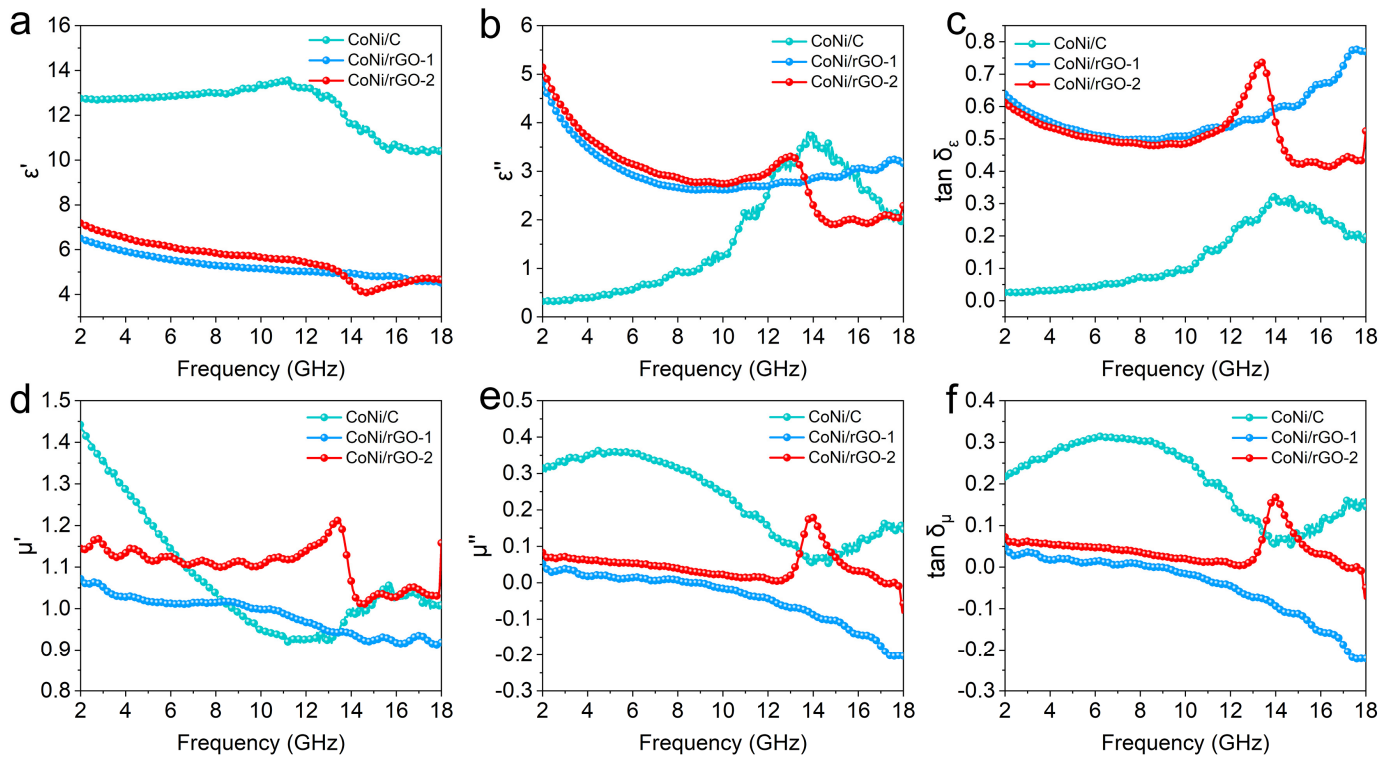


Figure 6. Electromagnetic parameters of CoNi/C, CoNi/rGO-1, and CoNi/rGO-2. (a) The real part (ϵ') and (b) the imaginary part (ϵ'') of the complex permittivity. (c) Dielectric loss tangents. (d) The real part (μ') and (e) the imaginary part (μ'') of the complex permeability. (f) Magnetic loss tangents.

4. Conclusions

In summary, bimetallic MOF-derived CoNi/rGO composites are successfully synthesized by a thermal reduction method. The electromagnetic parameters of the composite can be adjusted by tuning the ratio of GO in the precursors, resulting in the composites with both good impedance matching and excellent electromagnetic wave absorption performance. As a result, the CoNi/rGO-2 delivers optimal absorption performance with an RL_{\min} of -66.2 dB at 7.6 GHz. Moreover, the CoNi/rGO-2 can reach a maximum EAB of 6.8 GHz at 2.5 mm, mostly covering the entire Ku band and a portion of the X band. Excellent absorption performance can be attributed to the high magnetic loss from the CoNi alloy. Additionally, the introduction of rGO reduces the weight of the material and improves the dielectric loss and impedance matching of the composite. This work provides a method for the preparation of high-efficiency MOF-derived absorbers.

Author Contributions: Conceptualization, Data curation, Validation, Formal analysis, Methodology, Investigation, Writing—original draft, H.X.; Methodology, Formal analysis, Writing—review and editing, J.L.; Investigation, Y.Z.; Methodology, J.Y.; Resources, Project administration, T.W.; Resources, Project administration, Writing—review and editing, Q.W. All authors have read and agreed to the published version of the manuscript.

Funding: This work was supported by the Science and Technology Foundation of Lanzhou (2021-1-40), the Central Guidance on Local Science and Technology Development Fund of Gansu Province (23ZYQA314), and the LICP Cooperation Foundation for Young Scholars (HZJJ23-10).

Institutional Review Board Statement: Not applicable.

Informed Consent Statement: Not applicable.

Data Availability Statement: The raw data supporting the conclusions of this article will be made available by the authors on request.

Conflicts of Interest: The authors declare no conflicts of interest.

References

1. Li, Y.; Liu, X.; Nie, X.; Yang, W.; Wang, Y.; Yu, R.; Shui, J. Multifunctional organic-inorganic hybrid aerogel for self-cleaning, heat-insulating, and highly efficient microwave absorbing material. *Adv. Funct. Mater.* **2019**, *29*, 1807624. [[CrossRef](#)]
2. Sun, H.; Che, R.; You, X.; Jiang, Y.; Yang, Z.; Deng, J.; Qiu, L.; Peng, H. Cross-stacking aligned carbon-nanotube films to tune microwave absorption frequencies and increase absorption intensities. *Adv. Mater.* **2014**, *26*, 8120–8125. [[CrossRef](#)]
3. Bao, Y.; Guo, S.; Wang, W.; Qi, X.; Jia, Z.; Guan, H. Heterogeneous burr-like $\text{CoNiO}_2/\text{Ti}_3\text{C}_2\text{T}_x$ MXene nanospheres for ultralow microwave absorption and satellite skin application. *Chem. Eng. J.* **2023**, *473*, 145409. [[CrossRef](#)]
4. Qiu, Y.; Yang, H.; Hu, F.; Lin, Y. Two-dimensional CoNi @mesoporous carbon composite with heterogeneous structure toward broadband microwave absorber. *Nano Res.* **2022**, *15*, 7769–7777. [[CrossRef](#)]
5. Wang, R.; He, M.; Zhou, Y.; Nie, S.; Wang, Y.; Liu, W.; He, Q.; Wu, W.; Bu, X.; Yang, X. Self-assembled 3D flower-like composites of heterobimetallic phosphides and carbon for temperature-tailored electromagnetic wave absorption. *ACS Appl. Mater. Interfaces* **2019**, *11*, 38361–38371. [[CrossRef](#)]
6. Quan, B.; Liang, X.; Ji, G.; Zhang, Y.; Xu, G.; Du, Y. Cross-linking-derived synthesis of porous $\text{Co}_x\text{Ni}_y/\text{C}$ nanocomposites for excellent electromagnetic behaviors. *ACS Appl. Mater. Interfaces* **2017**, *9*, 38814–38823. [[CrossRef](#)] [[PubMed](#)]
7. Zou, Y.; Huang, X.; Fan, B.; Liu, Y.; Yue, J. Triple-layer structure of carbon foam coated with carbon nanotubes and FeNi alloy for high-performance electromagnetic wave absorption. *J. Alloys Compd.* **2023**, *946*, 169404. [[CrossRef](#)]
8. Chen, Z.; Tian, K.; Zhang, C.; Shu, R.; Zhu, J.; Liu, Y.; Huang, Y.; Liu, X. In-situ hydrothermal synthesis of NiCo alloy particles@hydrophilic carbon cloth to construct corn-cob-like heterostructure for high-performance electromagnetic wave absorbers. *J. Colloid Interface Sci.* **2022**, *616*, 823–833. [[CrossRef](#)]
9. Zhang, H.; Zhao, Y.; Zuo, X.; Huang, H.; Sun, C.; Fan, Z.; Pan, L. Construction of chiral-magnetic-dielectric trinity composites for efficient microwave absorption with low filling ratio and thin thickness. *Chem. Eng. J.* **2023**, *467*, 143414. [[CrossRef](#)]
10. Liu, Q.; Cao, Q.; Bi, H.; Liang, C.; Yuan, K.; She, W.; Yang, Y.; Che, R. $\text{CoNi@SiO}_2/\text{TiO}_2$ and CoNi@Air@TiO_2 microspheres with strong wideband microwave absorption. *Adv. Mater.* **2016**, *28*, 486–490. [[CrossRef](#)]
11. Aslam, M.A.; Ahsen, R.; Uddin, W.; ur Rehman, S.; Khan, M.S.; Bilal, M.; Li, N.; Wang, Z. Tailoring the morphology of CoNi alloy by static magnetic field for electromagnetic wave absorption. *Eur. Phys. J. Plus.* **2022**, *137*, 480. [[CrossRef](#)]
12. Qiu, H.; Zhu, X.; Chen, P.; Liu, J.; Zhu, X. Self-etching template method to synthesize hollow dodecahedral carbon capsules embedded with Ni-Co alloy for high-performance electromagnetic microwave absorption. *Compos. Commun.* **2020**, *20*, 100354. [[CrossRef](#)]
13. Tao, J.; Tan, R.; Xu, L.; Zhou, J.; Yao, Z.; Lei, Y.; Chen, P.; Li, Z.; Ou, J.Z. Ion-exchange strategy for metal-organic frameworks-derived composites with tunable hollow porous and microwave absorption. *Small Methods* **2022**, *6*, 2200429. [[CrossRef](#)] [[PubMed](#)]
14. Cheng, R.; Wang, Y.; Di, X.; Lu, Z.; Wang, P.; Ma, M.; Ye, J. Construction of MOF-derived plum-like NiCo@C composite with enhanced multi-polarization for high-efficiency microwave absorption. *J. Colloid Interface Sci.* **2022**, *609*, 224–234. [[CrossRef](#)]
15. Wu, F.; Ling, M.; Wan, L.; Liu, P.; Wang, Y.; Zhang, Q.; Zhang, B. Three-dimensional FeM₂Zn (M = Co or Ni) MOFs: Ions coordinated self-assembling processes and boosting microwave absorption. *Chem. Eng. J.* **2022**, *435*, 134905. [[CrossRef](#)]
16. Liu, J.; Jia, Z.; Zhou, W.; Liu, X.; Zhang, C.; Xu, B.; Wu, G. Self-assembled MoS_2 /magnetic ferrite CuFe_2O_4 nanocomposite for high-efficiency microwave absorption. *Chem. Eng. J.* **2022**, *429*, 132253. [[CrossRef](#)]
17. He, W.; Zheng, J.; Dong, W.; Jiang, S.; Lou, G.; Zhang, L.; Du, W.; Li, Z.; Li, X.; Chen, Y. Efficient electromagnetic wave absorption and Joule heating via ultra-light carbon composite aerogels derived from bimetal-organic frameworks. *Chem. Eng. J.* **2023**, *459*, 141677. [[CrossRef](#)]
18. Wu, Q.; Wang, B.; Fu, Y.; Zhang, Z.; Yan, P.; Liu, T. MOF-derived Co/CoO particles prepared by low temperature reduction for microwave absorption. *Chem. Eng. J.* **2021**, *410*, 128378. [[CrossRef](#)]
19. Liu, P.; Gao, S.; Zhang, G.; Huang, Y.; You, W.; Che, R. Hollow engineering to Co@N-doped carbon nanocages via synergistic protecting-etching strategy for ultrahigh microwave absorption. *Adv. Funct. Mater.* **2021**, *31*, 2102812. [[CrossRef](#)]
20. Sultanov, F.; Daulbayev, C.; Bakbolat, B.; Daulbayev, O. Advances of 3D graphene and its composites in the field of microwave absorption. *Adv. Colloid Interface Sci.* **2020**, *285*, 102281. [[CrossRef](#)]
21. Liang, X.; Quan, B.; Sun, B.; Man, Z.; Xu, X.; Ji, G. Extended effective frequency of three-dimensional graphene with sustainable energy attenuation. *ACS Sustain. Chem. Eng.* **2019**, *7*, 10477–10483. [[CrossRef](#)]

22. Liang, X.; Quan, B.; Ji, G.; Liu, W.; Zhao, H.; Dai, S.; Lv, J.; Du, Y. Tunable dielectric performance derived from the metal-organic framework/reduced graphene oxide hybrid with broadband absorption. *ACS Sustain. Chem. Eng.* **2017**, *5*, 10570–10579. [[CrossRef](#)]
23. Khanahmadi, S.; Masoudpanah, S.M. In-situ synthesis of NiCo/(Ni,Co)O/(Ni,Co)Fe₂O₄ composite as high-performance microwave absorber. *J. Mater. Res. Technol.* **2023**, *22*, 585–595. [[CrossRef](#)]
24. Zhao, B.; Li, Y.; Zeng, Q.; Wang, L.; Ding, J.; Zhang, R.; Che, R. Galvanic replacement reaction involving core-shell magnetic chains and orientation-tunable microwave absorption properties. *Small* **2020**, *16*, 2003502. [[CrossRef](#)] [[PubMed](#)]
25. Wang, Y.-L.; Wang, G.-S.; Zhang, X.-J.; Gao, C. Porous carbon polyhedrons coupled with bimetallic CoNi alloys for frequency selective wave absorption at ultralow filler loading. *J. Mater. Sci. Technol.* **2022**, *103*, 34–41. [[CrossRef](#)]
26. Zhang, N.; Huang, Y.; Zong, M.; Ding, X.; Li, S.; Wang, M. Synthesis of ZnS quantum dots and CoFe₂O₄ nanoparticles co-loaded with graphene nanosheets as an efficient broad band EM wave absorber. *Chem. Eng. J.* **2017**, *308*, 214–221. [[CrossRef](#)]
27. Zhang, X.; Tian, X.; Qiao, J.; Fang, X.; Liu, K.; Liu, C.; Lin, J.; Li, L.; Liu, W.; Liu, J.; et al. In-situ fabrication of sustainable-N-doped-carbon-nanotube-encapsulated CoNi heterogenous nanocomposites for high-efficiency electromagnetic wave absorption. *Small* **2023**, *19*, 2302686. [[CrossRef](#)] [[PubMed](#)]
28. Lv, Y.; Tian, J.; Chen, Z.; Wang, J.; Ma, L.-A.; Zhang, L.; Chen, S.; Wang, Q.; Ye, X. MXene/bimetallic CoNi-MOF derived magnetic-dielectric balanced composites with multiple heterogeneous interfaces for excellent microwave absorption. *Chem. Eng. J.* **2023**, *478*, 147413. [[CrossRef](#)]
29. Chen, B.; Yun, J.; Zhao, Y.; Liu, Z.; Yan, J.; Deng, Z.; Zhang, H.; Zhao, W.; Wang, G.; Zhang, J. Constructing multiple heterogeneous interfaces in porous bimetallic FeNi₃/C and CoNi/C flowers towards brilliant electromagnetic wave absorption performance. *Carbon* **2023**, *212*, 118108. [[CrossRef](#)]
30. Yu, G.; Ye, M.; Han, A.; Liu, Q.; Su, Y.; Chen, C. Optimization of electromagnetic wave absorption properties of CoNi/MoSe₂ composites with 3D flower-like by controlling the Co/Ni molar ratio. *J. Alloys Compd.* **2023**, *939*, 168592. [[CrossRef](#)]
31. He, N.; He, Z.; Liu, L.; Lu, Y.; Wang, F.; Wu, W.; Tong, G. Ni²⁺ guided phase/structure evolution and ultra-wide bandwidth microwave absorption of Co_xNi_{1-x} alloy hollow microspheres. *Chem. Eng. J.* **2020**, *381*, 122743. [[CrossRef](#)]
32. Liang, L.-L.; Liu, Z.; Xie, L.-J.; Chen, J.-P.; Jia, H.; Kong, Q.-Q.; Sun, G.-H.; Chen, C.-M. Bamboo-like N-doped carbon tubes encapsulated CoNi nanospheres towards efficient and anticorrosive microwave absorbents. *Carbon* **2021**, *171*, 142–153. [[CrossRef](#)]
33. Wang, W.; Nan, K.; Zheng, H.; Li, Q.; Wang, Y. Ion-exchange reaction construction of carbon nanotube-modified CoNi/MoO₂/C composite for ultra-intense and broad electromagnetic wave absorption. *Carbon* **2023**, *210*, 118074. [[CrossRef](#)]
34. Liu, Y.; Zhang, X.; Chen, X.; Wu, Y.; Zhang, C.; Wang, J.; Ji, J.; Li, K. Intense nonlinear dielectric and magnetic resonances of core-shell Ni@graphene composites and their improved microwave absorption properties. *J. Mater. Chem. C.* **2021**, *9*, 4910–4920. [[CrossRef](#)]
35. Miao, P.; Qu, N.; Chen, W.; Wang, T.; Zhao, W.; Kong, J. A two-dimensional semiconductive Cu-S metal-organic framework for broadband microwave absorption. *Chem. Eng. J.* **2023**, *454*, 140445. [[CrossRef](#)]
36. Ma, Q.; Qiang, R.; Shao, Y.; Yang, X.; Xue, R.; Chen, B.; Chen, Y.; Feng, S. MOF-derived Co-C composites with 3D star structure for enhanced microwave absorption. *J. Colloid Interface Sci.* **2023**, *651*, 106–116. [[CrossRef](#)] [[PubMed](#)]
37. Wu, F.; Wan, L.; Li, Q.; Zhang, Q.; Zhang, B. Ternary assembled MOF-derived composite: Anisotropic epitaxial growth and microwave absorption. *Compos. Part B Eng.* **2022**, *236*, 109839. [[CrossRef](#)]
38. Wang, L.; Wen, B.; Yang, H.; Qiu, Y.; He, N. Hierarchical nest-like structure of Co/Fe MOF derived CoFe@C composite as wide-bandwidth microwave absorber. *Compos. Part A Appl. Sci. Manuf.* **2020**, *135*, 105958. [[CrossRef](#)]
39. Jiang, R.; Wang, Y.; Wang, J.; He, Q.; Wu, G. Controlled formation of multiple core-shell structures in metal-organic frame materials for efficient microwave absorption. *J. Colloid Interface Sci.* **2023**, *648*, 25–36. [[CrossRef](#)] [[PubMed](#)]
40. Hu, Q.; Yang, R.; Yang, S.; Huang, W.; Zeng, Z.; Gui, X. Metal-organic framework-derived core-shell nanospheres anchored on Fe-filled carbon nanotube sponge for strong wideband microwave absorption. *ACS Appl. Mater. Interfaces* **2022**, *14*, 10577–10587. [[CrossRef](#)] [[PubMed](#)]
41. Wu, F.; Li, Q.; Liu, Z.; Shah, T.; Ahmad, M.; Zhang, Q.; Zhang, B. Fabrication of binary MOF-derived hybrid nanoflowers via selective assembly and their microwave absorbing properties. *Carbon* **2021**, *182*, 484–496. [[CrossRef](#)]
42. Bi, Y.; Ma, M.; Liu, Y.; Tong, Z.; Wang, R.; Chung, K.L.; Ma, A.; Wu, G.; Ma, Y.; He, C.; et al. Microwave absorption enhancement of 2-dimensional CoZn/C@MoS₂@PPy composites derived from metal-organic framework. *J. Colloid Interface Sci.* **2021**, *600*, 209–218. [[CrossRef](#)]
43. Wang, L.; Yu, X.; Li, X.; Zhang, J.; Wang, M.; Che, R. MOF-derived yolk-shell Ni@C@ZnO Schottky contact structure for enhanced microwave absorption. *Chem. Eng. J.* **2020**, *383*, 123099. [[CrossRef](#)]
44. Xu, H.; Zhang, G.; Wang, Y.; Ning, M.; Ouyang, B.; Zhao, Y.; Huang, Y.; Liu, P. Size-dependent oxidation-induced phase engineering for MOFs derivatives via spatial confinement strategy toward enhanced microwave absorption. *Nano-Micro Lett.* **2022**, *14*, 102. [[CrossRef](#)] [[PubMed](#)]
45. Ding, Z.; Du, Z.; Liu, Y.; Zhang, Q.; Zhao, Z.; Hou, M.; Wang, X.; Hassan, Y.A.; Huang, X.; Yue, J.; et al. Reduced graphene oxide loaded with rich defects CoO/Co₃O₄ for broadband microwave absorption. *Compos. Part B Eng.* **2023**, *249*, 110403. [[CrossRef](#)]
46. Zhao, T.; Liu, Y.; Wan, H.; Li, Z.; Wu, Y.; Yan, H. Electromagnetic wave absorption properties of carbon-encapsulated Co-Cu alloy nanoparticles prepared by gas explosion. *Mater. Chem. Phys.* **2023**, *310*, 128486. [[CrossRef](#)]

47. Zhou, Y.; Song, X.; Yan, S.; Ni, C.; Xu, L.; Yu, L.; Li, X. A hierarchical CoNi@nitrogen doped C/macroporous C composite derived from a new bimetallic MOF and *Juncus effusus* as a broadband electromagnetic wave absorber. *J. Alloys Compd.* **2023**, *944*, 169146. [[CrossRef](#)]
48. Wang, H.; Meng, F.; Huang, F.; Jing, C.; Li, Y.; Wei, W.; Zhou, Z. Interface modulating CNTs@PANi hybrids by controlled unzipping of the walls of CNTs to achieve tunable high-performance microwave absorption. *ACS Appl. Mater. Interfaces* **2019**, *11*, 12142–12153. [[CrossRef](#)]

Disclaimer/Publisher’s Note: The statements, opinions and data contained in all publications are solely those of the individual author(s) and contributor(s) and not of MDPI and/or the editor(s). MDPI and/or the editor(s) disclaim responsibility for any injury to people or property resulting from any ideas, methods, instructions or products referred to in the content.